Residual-resistivity anisotropy in potassium

Marilyn F. Bishop and A. W. Overhauser

Department of Physics, Purdue University, West Lafayette, Indiana 47907
(Received 23 March 1978)

We present evidence from induced-torque measurements of Holroyd and Datars supporting an anisotropy in the residual resistivity of potassium of about five to one and argue against explanation of their data by extrinsic mechanisms. We explain how the hypothesis that the conduction electrons are in a static charge-density-wave state leads naturally to the prediction of a large residual resistivity anisotropy. Resistivity calculations are performed using several model impurity-scattering potentials. Numerical results are presented for parameters characteristic of potassium, yielding anisotropies as large as four to one. We suggest that induced-torque experiments might be used to determine whether a given potassium sample has a single charge-density-wave domain and encourage that de Haas–van Alphen experiments be performed on such "single-domain" samples.

I. INTRODUCTION

Reports of a giant torque anomaly in potassium have generated considerable controversy in recent years. Potassium is generally considered to be of cubic symmetry and, according to most textbook descriptions, to be an example of a nearly-free-electron metal. Within this simple picture, the induced torque in spherical samples of potassium is expected to be independent of magnetic field direction. For this reason, the large anisotropies observed originally by Schaefer and Marcus[1] at 4 K in hundreds of spherical samples of potassium created a severe dilemma. A four-peaked pattern of twofold symmetry that contradicted the cubic symmetry of the metal appeared in the induced torque. Earlier, Lass had measured the induced torque in one large spherical sample and had found the results to be independent of magnetic field direction.[2] In response to the anisotropies, he suggested that the observations could be explained if the samples were sufficiently non-spherical,[3] except that torque data at 80 K showed that most samples were essentially undistorted.

In response to these conflicting reports, Holroyd and Datars[4] decided to test the dependence of results on methods of preparation of samples of potassium. They were able to reproduce results of both groups in a controlled manner. In addition, for some samples, they found torque anisotropies larger than those seen by Schaefer and Marcus, and in one particular sample, nearly an order of magnitude larger. No theoretical explanation was given for the observed dependences on sample preparation.

In this paper, we will concentrate on the results, shown in Fig. 1, of the sample for which the most bizarre induced-torque effects were observed. For this specimen, sample K-10 of Holroyd and

Datars, the four-peaked pattern for the largest magnetic fields used exhibited an anisotropy of 45 to one, while this pattern at low fields became two-peaked, with the old minima becoming the new maxima and minima. This anisotropy, extrapolated to zero field, is about three to one, implying that the residual resistivity of potassium has an anisotropy of about five to one, as we shall see in Sec. II. The purpose of this paper is to present a possible interpretation of this resistivity anisotropy. We will show that the assumption that the conduction electrons in potassium are in a static charge-density-wave state is consistent with the observed residual resistivity anisotropy.[5] We make no attempt here to explain the exotic high-field behavior.

The organization of the paper is as follows. In Sec. II, we discuss the induced-torque experiments and include data of Holroyd and Datars. In addition, we consider the possibilities of extrinsic mechanisms explaining the observed anomalies. In Sec. III, we explicate the relevant properties of charge-density waves. In Sec. IV, we introduce the model impurity scattering potentials to be used for the residual resistivity calculation of Sec. V and for the numerical predictions of Sec. VI. Finally, in Sec. VII we present the conclusions.

II. INDUCED-TORQUE EXPERIMENTS

Induced-torque experiments are performed by suspending a sample, usually spherical in shape, in a slowly rotating magnetic field. Because the field varies in time, currents are induced that interact with the magnetic field to exert a torque on the sample. This torque is measured as a function of both the direction and magnitude of the magnetic field. The induced torque in a spherical sample of a simple metal, i.e., a metal with

a spherical Fermi surface, should be independent
of the orientation of the magnetic field. For a co-
ordinate system in which the axis of rotation is
along y and the magnetic field of constant magni-
tude B is along z, the torque induced is in the y
direction and is given by[6-8]

$$N_y = \frac{2\pi R^5}{15} \Omega n^2 e^2 \rho_0 \frac{(\omega_c \tau)^2}{1+(\frac{1}{2}\omega_c \tau)^2} , \qquad (2.1)$$

where R is the radius of the sphere, Ω is the ro-
tation speed of the magnet, n is the electron den-
sity, ω_c ($=eB/mc$) is the cyclotron frequency,
τ is the relaxation time, and ρ_0 is the resistivity.
While de Haas–van Alphen measurements on po-
tassium seem to indicate that its Fermi surface is
spherical to within 0.1%,[9] gigantic anisotropies
are observed in induced-torque experiments, which
are in conflict with this simple model.

In order to study explicitly the results of induced-
torque experiments, we refer to the data for sam-
ple K-10 of Holroyd and Datars[4] in Fig. 1. This
specimen exhibits an anisotropy that is nearly an
order of magnitude larger than that observed on
any other sample ever studied and is therefore an
excellent example of the effects that we wish to
discuss in this paper. The induced torque is
plotted versus orientation of the magnetic field
for various field strengths, with torque an in-

creasing function fo field. In Fig. 1(a), field val-
ues are for 500 G and from 1 to 17 kG in steps
of 1 kG. In Fig. 1(b), field values are for 1–23 kG
in steps of 1 kG. The magnetic field was rotated
at a speed of 22°/min for axes of rotation along the
growth axis [Fig. 1(a)] and perpendicular to the
growth axis [Fig. 1(b)]. The temperature of the
sample was kept at 1.5 K during experiments. In
order to guarantee a precise shape for the sam-
ple, the potassium was grown in a kel-F mold
with a spherical cavity of diameter of 1.11 cm,
machined to within 10^{-3} in.[4] The angular depen-
dence in Fig. 1(a), obtained when the magnetic
field was rotated in a plane perpendicular to the
growth axis, is essentially isotropic and is thus
in agreement with the behavior expected from a
free-electron metal, as given in Eq. (2.1). On the
contrary, an anomalous four-peaked anisotropy
of 45 to one appears in the torque pattern for high
fields for the case in which the growth axis was in
the plane of rotation, as in Fig. 1(b). The magni-
tudes of these peaks decrease with respect to the
minima when the strength of the field is reduced,
until at low fields, the four minima become the new
maxima and minima of a two-peaked pattern. For
this case, the dips occur for the field along the
growth axis and the peaks for the field perpen-
dicular to the growth axis. As a consequence of
these orientational dependences, the growth axis
emerges as a preferred direction in this specimen.
Thus potassium must be electrically uniaxial and
not cubic. Unfortunately, the sample orientation
was not determined by a diffraction experiment.
However, it is known that K films grown on smooth,
amorphous substrates have a [110] direction per-
pendicular to the surface.[10] Therefore, since the
nucleation of the crystal was at the bottom of a
smooth spherical mold, it is probable that the
growth axis was along some [110] direction.

According to the Lifshitz-Azbel-Kaganov (LAK)
transport theorems,[11] a metal with a single, sim-
ply-connected Fermi surface must have a re-
sistivity $\rho(B)$ independent of field B at high fields,
i.e., $\omega_c \tau \gg 1$. Since the torque depends on this
magnetoresistance, it too must saturate. In fact,
for the sample of Fig. 1, the torque at the peaks
should have stopped increasing at about 1 or 2
kG, yet it continues to increase even at 23 kG.
Thus, the torque patterns prove in addition that
the Fermi surface of K is multiply connected.
This is in direct contradiction with de Haas–van
Alphen measurements.[9]

In this paper we will not attempt to explain the
high-field torque patterns and instead turn our
attention to the low-field results. The low magnet
rotation rate makes the method nearly a dc mea-
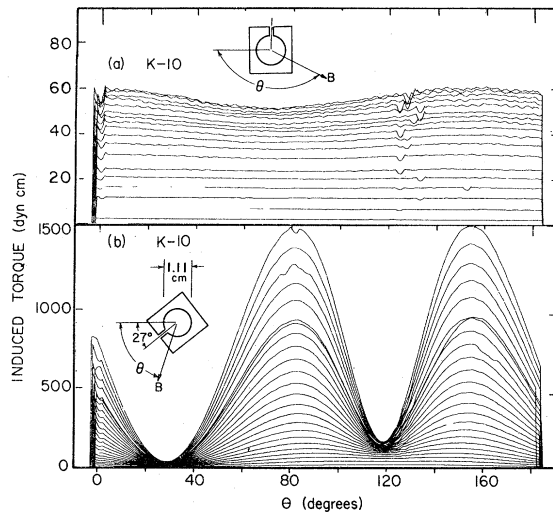surement. In order to examine the relevant data

FIG. 1. Induced-torque vs magnetic field direction
for several field values for sample K-10 of Holroyd and
Datars, which was prepared in a mold. The sample was
a sphere of diameter 1.11 cm. (a) The field was rotated
about the growth axis and the magnitude of the field was
500 G for the lowest curve and ranged from 1 to 17 kG,
in steps of 1 kG, for the higher curves. (b) The field
was rotated in a plane containing the growth axis, with
magnitudes ranging from 1 to 23 kG, in steps of 1 kG.

in more detail, we plot with circles in Fig. 2 the induced torque at 28°, or at the minimum in Fig. 1(b) (lower curve), and at 118° (middle curve) versus magnetic field. The upper circles at given fields are ratios of the corresponding points in the lower two curves and thus give the torque anisotropy. Solid curves are drawn through the data,

with dashed curves possible extensions of the ratio to zero field. Therefore, we estimate the zero-field limit of the torque anisotropy to be between 2.5 and 3 to 1. If a sample is completely spherical an induced-torque anisotropy can result only if the resistivity tensor $\bar{\rho}$ of the metal is not isotropic. In general, the expression for the torque

N_y induced in a sphere is given by[7,8]:

$$N_y = \frac{4\pi(15c^2)^{-1}R^5 B^2 \Omega \lambda}{\lambda(\rho_{yy}+\rho_{zz}) - (\rho_{xx}+\rho_{zz})\rho_{xz}\rho_{zx} - (\rho_{xx}+\rho_{yy})\rho_{xy}\rho_{yx} - \rho_{xy}\rho_{yz}\rho_{zx} - \rho_{xz}\rho_{zy}\rho_{yx}} , \tag{2.2a}$$

where

$$\lambda \equiv (\rho_{xx}+\rho_{zz})(\rho_{xx}+\rho_{yy}) - \rho_{yz}\rho_{zy} . \tag{2.2b}$$

Here, the $\{\rho_{ij}\}$ are elements of $\bar{\rho}$. The magnetic field $\vec{B}$ is assumed to be in the z direction with axis of rotation along y.

For sample K-10 of Holroyd and Datars, for which the growth axis was determined from Figs. 1 and 2 to be a preferred direction in the specimen, the zero-field resistivity tensor $\bar{\rho}$ is diagonal in a coordinate system in which the growth axis is along any Cartesian axis. The resistivities parallel and perpendicular to the growth axis are given by $\gamma\rho_0$ and ρ_0, respectively. For low fields, we use the resistivity tensor that includes the Hall effect. If the growth axis is along $\hat{x}$ and $\vec{B}$ along

$\hat{z}$, the resistivity tensor for low fields is given by

$$\bar{\rho} = \rho_0 \begin{pmatrix} \gamma & \omega_c \tau & 0 \\ -\omega_c \tau & 1 & 0 \\ 0 & 0 & 1 \end{pmatrix}, \tag{2.3}$$

where $\rho_0 \omega_c \tau = B/nec$ and $\rho_0 = m/ne^2\tau$. From Eq. (2.2), we obtain the torque along $\hat{y}$ for this case,

$$N_y^{(1)} = \frac{4\pi R^5 B^2 \Omega}{15c^2\rho_0} \frac{(1+\gamma)^2}{2(1+\gamma)^2 + (1+\gamma)(\omega_c\tau)^2} . \tag{2.4}$$

For a second case with the growth axis and $\vec{B}$ both along $\hat{z}$, the resistivity tensor is

$$\bar{\rho} = \rho_0 \begin{pmatrix} 1 & \omega_c \tau & 0 \\ -\omega_c \tau & 1 & 0 \\ 0 & 0 & \gamma \end{pmatrix}. \tag{2.5}$$

The torque along $\hat{y}$ is then

$$N_y^{(2)} = \frac{4\pi R^5 B^2 \Omega}{15c^2\rho_0} \frac{2(1+\gamma)}{2(1+\gamma)^2 + 2(\omega_c\tau)^2} . \tag{2.6}$$

From Eqs. (2.4) and (2.6), we may find the ratio $\Re$ between $N_y^{(1)}$ and $N_y^{(2)}$, or the torque anisotropy for low fields,

$$\Re = \frac{(1+\gamma)^2 + (\omega_c\tau)^2}{2(1+\gamma) + (\omega_c\tau)^2} . \tag{2.7}$$

In the limit of zero field, $\omega_c = 0$, and the expression reduces to

$$\Re = \tfrac{1}{2}(\gamma + 1) . \tag{2.8}$$

Since $\Re$ in this limit is between 2.5 and 3, γ must be between 4 and 5. This is consistent with the value $\gamma = 4$ that was originally estimated from the data of Schaefer and Marcus.[8] From the data in Figs. 1 and 2, we find that $\omega_c\tau \sim 2.5$ at 1 kG, implying that $\tau \sim 1.4 \times 10^{-10}$ sec, for the directions
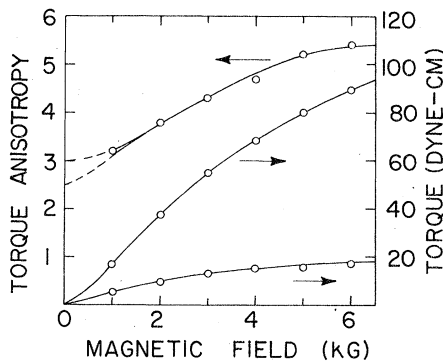

FIG. 2. Low-magnetic-field values of induced torque shown in Fig. 1, with data points plotted in circles. The lower curve is the minimum in induced torque taken at an angle $\theta = 28°$ in Fig. 1, while the middle curve is taken at $\theta = 118°$. The upper curve is the ratio of these limiting values and is the low-field-torque anisotropy. Solid curves are drawn through the experimental points, and the dashed curves are reasonable extrapolations of the anisotropy to zero field.

perpendicular to the growth axis. Along the growth axis, $\omega_c \sim 0.5$ or $\tau \sim 2.8 \times 10^{-11}$ sec.

The anisotropy versus field in Fig. 2 increases with increasing field, unlike Eq. (2.7), which decreases. This is probably a manifestation of high-field effects, which are not explained in this paper. Nevertheless, Eq. (2.7) can provide some theoretical basis for the extrapolation procedure. Certainly one cannot easily extrapolate the torque curves themselves to zero, since they must vary according to B^2 as $B \to 0$. The ratio removes this dependence, so that the reasonable curve to extrapolate is that showing the anisotropy. Suppose that one tried to extrapolate this curve to unity, i.e., $\mathfrak{R} \to 1$ as $B \to 0$. This means that $\gamma = 1$ at $B = 0$, as can be seen from Eq. (2.8). Since $\mathfrak{R} \approx 3$ at $B = 1$ kG, then it must be true that $\gamma \sim 6$ at 1 kG [Eq. (2.7)]. Therefore, this requires a 500% magnetoresistance along the growth axis for 1 kG. However, the observed magnetoresistance in po-

tassium is typically 2% for 1 kG.

The postulation of an oriented array of dislocations arising from unusual strain patterns in a sample could lead to a resistivity that is not isotropic. Strains in samples of interest can be estimated to be on the order of a percent. Jones found the residual resistance ratio in potassium wires to decrease linearly by 1.3% per percent longitudinal strain.[12] Thus, the value of $(\gamma - 1)$ determined from a dislocation model could be at most a few percent, or orders of magnitude smaller than that observed.

As an alternative to the above discussion, Lass[3] has suggested that the data of Schaefer and Marcus could be explained within the model of an isotropic resistivity tensor if the samples had been nonspherical by 10%–15%. The model that he proposed was that of an ellipsoid of revolution with the radius along the axis of the ellipsoid a fraction of the radius R perpendicular to the axis.

The induced torque is then given by[3]

$$N_y = \frac{2\pi}{15c^2}\sigma B^2 \Omega R^5 \eta \left(\frac{1 - E + E \sin^2\beta \sin^2\theta + (\omega_c\tau)^2 E^2 \sin^4\beta \sin^2\theta \cos^2\theta}{1 + \frac{1}{4}(\omega_c\tau)^2[1 - E + E(3 + E) \sin^2\beta \cos^2\theta]} \right),$$

(2.9)

where β is the angle between the axis of the ellipse and the y direction, and θ is the angle between the magnetic field direction $\vec{B}$ and the projection of the axis of the ellipse onto the x-z plane. $\sigma = ne^2\tau/m$ is the electrical conductivity and $E = (1 - \eta^2)/(1 + \eta^2)$ is an asymmetry parameter. With $\eta \approx 0.9$, Lass was able to produce curves similar to those of Schaefer and Marcus. However, the deviations from sphericity were determined experimentally to be 2% or less by performing torque measurements at 80 °K, or for $\omega_c\tau \ll 1$.

An even greater difficulty with this explanation arises in the consideration of the results of sample K-10 of Holroyd and Datars, given here in Figs. 1 and 2. The torque anisotropy at low fields could be reproduced by Lass's model [Eq. (2.9)] if $\eta \approx 0.45$, supposing that the mold had been only about half filled.[13] Nevertheless, this could not possibly explain the data. For a magnetic field of 1 kG, the torque calculated from Eq. (2.4) with $\beta = \frac{1}{2}\pi$ and $\theta = 0$, corresponding to the minimum in the angular pattern in Fig. 1(b) (28° in that figure), could never exceed 3.2 dyn cm, regardless of relaxation time τ. The torque of 5.4 dyn cm observed by Holroyd and Datars is therefore much too large to be consistent with this explanation,

implying that the mold had to be filled. The exceedingly unlikely possibility that a planar crack developed in the sample perpendicular to the growth axis could remove this objection. The two equal hemispheres thus produced could be represented by two ellipsoids with $\eta \approx 0.5$, yielding twice the torque of a half-filled mold. On the other hand, even this hypothesis cannot provide a satisfactory explanation of the data. If in Eq. (2.9), $\beta = \frac{1}{2}\pi$ and $E \approx 0.5$, the appropriate value of $\omega_c\tau$ is determined by the criterion that the angular pattern in θ remain two peaked through a magnetic field strength of 2 kG and begin the four-peaked behavior by 3 kG. However, this choice, $\omega_c\tau \approx 1.8$ causes the ratio $\mathfrak{R}$ to be more than 50% too large. In addition, an enormous Kohler slope, larger than 0.12, is needed to fit the peaks at 23 kG. Unfortunately, with this value, the dips in the angular pattern no longer agree reasonably with experiment. Therefore, it is impossible to obtain legitimate agreement of the results of this model with the data in Figs. 1 and 2. We conclude, therefore, that the residual resistivity is indeed anisotropic and that Eqs. (2.2) are the corresponding expressions for the induced torque.

A search for an explanation of the residual re-

sistivity anomaly in potassium leads us to the supposition that the conduction electrons are in a static charge-density-wave state. Other alkalimetal anomalies have been explained as a result of this proposition.[14] As we shall show, this hypothesis provides a quantitative explanation for the anisotropy observed in the zero-field limit in sample K-10 by Holroyd and Datars. Although we have used the high-field induced-torque data in our arguments against proposed explanations by extrinsic mechanisms, we make no attempt here to explain the high-field anomalies.

III. CHARGE-DENSITY WAVES

For simplicity, since the effects of a lattice are not important here, we consider a jellium model in which the positive ions are replaced by a uniformly charged deformable jelly. Within the simple free-electron theory of metals, since the positive background is uniform, it is assumed that the electronic ground state will be that of a spatially uniform charge density. However, it has been shown that this is possibly not the case when electron-electron interactions are taken into account.[15] A symmetry-breaking instability can occur, leading to a spin-density-wave (SDW) or charge-density-wave (CDW) state. For alkali metals, theoretical arguments, coupled with experimental evidence, favor the CDW state.

A CDW is characterized by a periodic spatial modulation in electron charge density,

$$\rho(\vec{r}) = \rho_0 (1 - p\cos\vec{Q}\cdot\vec{r}), \qquad (3.1)$$

where $\vec{Q}$ and p are the wave vector and the fractional amplitude of the CDW, respectively. The positive background deforms in order to assure local-charge neutrality, with the static local displacement given by

$$\vec{u}(\vec{r}) = (p\vec{Q}/Q^2)\sin\vec{Q}\cdot\vec{r} . \qquad (3.2)$$

In the deformable jellium model, this adjustment incurs no energy penalty. Whether or not a particular real metal has a CDW ground state depends on how closely it resembles this model.

In alkali metals, the Born-Mayer ion-ion interactions are known to be extremely weak,[16] enabling the ions to displace easily from their equilibrium positions. The magnitude of $\vec{Q}$ is approximately the diameter of the Fermi surface, as will be discussed below. The lowest energy direction for $\vec{Q}$ is determined by that direction that minimizes the wave vector $\vec{Q}'$ of the static phonon of Eq. (3.2), given by[17]

$$\vec{Q}' = (2\pi/a)(1, 1, 0) - \vec{Q}, \qquad (3.3)$$

where a is the lattice constant of the bcc lattice.

Clearly, the favorable direction for $\vec{Q}$ is along the [110] direction. This is because any deformation energy associated with the neutralization of charge density in Eq. (3.1) by displacements in Eq. (3.2) should be proportional to the wave vector $\vec{Q}'$.

The spatial modulation of the electron density given in Eq. (3.1) will occur only if each electron experiences a sinusoidal potential. Such a potential arises self-consistently through exchange and correlation potentials of the electron gas. The one-electron Schrödinger equation incorporating these effects may be written

$$(p^2/2m + G\cos\vec{Q}\cdot\vec{r})\Psi_{\vec{k}} = E_{\vec{k}}\Psi_{\vec{k}}, \qquad (3.4)$$

The charge modulation of the electron gas occurs only if the periodic part G of the exchange and correlation potential is sufficiently large. However, the density modulation must be large enough to generate this periodic part of the potential. This process occurs in a self-consistent manner, requiring a $\vec{k}$ dependence of G. Solution of an integral equation for $G(\vec{k})$ is required. Since such analyses overly complicate the problem of interest, we approximate G as a constant, whose value is determined by experiments, assuming that such an assumption does not alter the principal features of our calculations.

Since Eq. (3.4) is the Mathieu equation, it does not have compact solutions. On the other hand, we obtain sufficient accuracy by dividing the periodic potential into two parts, one that leads to an energy gap at $k_z = -\frac{1}{2}Q$, and the other that leads to a gap at $k_z = \frac{1}{2}Q$. In the calculation of the residual resistivity, only the states below the gap need be considered. Near each gap, the energies and wave functions are significantly altered, requiring an accurate solution with degenerate first-order perturbation theory. First, we consider the case for $k_z \approx -\frac{1}{2}Q$ and assume that the perturbed state $|\vec{k}\rangle$ mixes with $|\vec{k}+\vec{Q}\rangle$ only. This leads to the secular equation

$$\begin{vmatrix} \epsilon_{\vec{k}} - E_{\vec{k}} & \frac{1}{2}G \\ \frac{1}{2}G & \epsilon_{\vec{k}+\vec{Q}} - E_{\vec{k}} \end{vmatrix} = 0, \qquad (3.5)$$

within the space defined by the basis set $|\vec{k}\rangle$ and $|\vec{k}+\vec{Q}\rangle$, where $\epsilon_{\vec{k}} = \hbar^2 k^2/2m$, the unperturbed energy of the state $|\vec{k}\rangle$. The energy for the solution below the gap is

$$E_{\vec{k}} = \frac{1}{2}(\epsilon_{\vec{k}} + \epsilon_{\vec{k}+\vec{Q}}) - \frac{1}{2}[(\epsilon_{\vec{k}} - \epsilon_{\vec{k}+\vec{Q}})^2 + G^2]^{1/2} . \qquad (3.6)$$

The corresponding eigenfunction is

$$\Psi_{\vec{k}} = \cos\xi e^{i\vec{k}\cdot\vec{r}} - \sin\xi e^{i(\vec{k}+\vec{Q})\cdot\vec{r}}, \qquad (3.7)$$
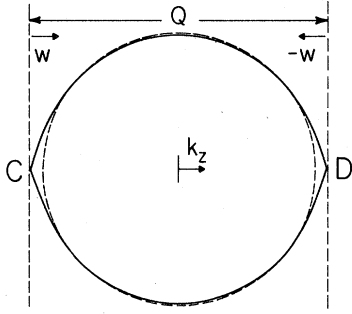
where

FIG. 3. Lime-shaped Fermi surface (solid curve) for a jellium model in which conduction electrons are in a CDW ground state with $G/E_F^0 = 0.5$. The dashed curve is that of the free-electron Fermi sphere of radius k_F, with the same volume as the lime. Points C and D, the conical points, are the regions of greatest deviation from the sphere.

$$\cos\xi(\vec{k}) = G/[G^2 + 4(\epsilon_{\vec{k}} - E_{\vec{k}})^2]^{1/2} . \qquad (3.8)$$

Far away from the gap, these solutions reduce to those found by nondegenerate perturbation theory. The CDW instability is optimized if the Fermi energy E_F lies in the CDW energy gap. This is accomplished if one requires critical contact between the Fermi surface and the two energy gaps of magnitude G. This implies that $Q \approx 2k_F$, or more precisely, that $\vec{Q}$ spans the Fermi surface. For $G = 0$, $Q = 2k_F$. The Fermi surface is distorted into the shape of a lime or lemon, as shown in Fig. 3. Here Q is the distance between the two conical points at $C(k_z = -\frac{1}{2}Q)$ and $D(k_z = +\frac{1}{2}Q)$.

We obtain the equation for the Fermi surface by setting

$$E_{\vec{k}} = E_F = \hbar^2(\tfrac{1}{2}Q)^2/2m - \tfrac{1}{2}G , \qquad (3.9)$$

which makes E_F the energy of the point of critical contact, point C in Fig. 3. We now choose $\vec{Q}$ in the z direction and introduce dimensionless variables, valid for $-\frac{1}{2}Q < k_z < 0$:

$$u = k_x/Q , \quad v = k_y/Q , \quad w = (k_z + \tfrac{1}{2}Q)/Q , \qquad (3.10)$$

so that in this coordinate system, the point C is at $(0, 0, 0)$. The equation of the Fermi surface in this system is given by

$$\kappa = (u^2 + v^2)^{1/2} = [(w^2 + \alpha^2)^{1/2} - w^2]^{1/2} , \qquad (3.11a)$$

where

$$\alpha \equiv mG/\hbar^2 Q^2 . \qquad (3.11b)$$

The above analysis applies only for the case $k_z < 0$, since for $k_z > 0$, the gap at point $D(k_z = \frac{1}{2}Q)$ in Fig. 3 becomes important. The expressions

for $0 < k_z < \frac{1}{2}Q$ may be obtained by replacing $\vec{Q}$ by $-\vec{Q}$ in Eqs. (3.4)–(3.6). The variables u, v, and κ are defined as before. In addition, if the dimensionless variable w is redefined as

$$w = (k_z + \tfrac{1}{2}Q)/Q , \quad k_z < 0 \qquad (3.12a)$$

$$w = (k_z - \tfrac{1}{2}Q)/Q , \quad k_z > 0 \qquad (3.12b)$$

then the equation for the Fermi surface, Eq. (3.10), applies for both regions of k_z. The definition (3.12b) corresponds to displacing the right half of the Fermi surface to the left $(-k_z)$ such that the two conical points touch. Then w ranges from $-\frac{1}{2}$ to $+\frac{1}{2}$. This is equivalent to considering the Fermi surface in a repeated-zone scheme.

The volume of the Fermi surface determines the number of electrons in the system. The value of Q is obtained by setting this volume equal to the volume of the Fermi surface when $G = 0$, or the volume of the free-electron sphere $\frac{4}{3}\pi k_F^3$. To first order in α, this yields:

$$Q \cong 2k_F(1 + G/4E_F^0) , \qquad (3.13)$$

where $E_F^0 = \hbar^2 k_F^2/2m$ is the free-electron Fermi energy, or the Fermi energy for $G = 0$. However, within this approximation, the volume within the Fermi surface does not remain constant as the value of G is increased to the largest value of G of interest here. In fact, for $G = 0.5E_F^0$, the volume was about 8% larger than that with $G = 0$, with the consequence that the number of electrons had increased by 8%. Since this is clearly unacceptable, we must include higher-order terms in Q. For consistency, we also include higher-order corrections to the energy and wave functions. In addition, we will write all expressions in a form valid for both $k_z < 0$ and $k_z > 0$ by using the dimensionless variables defined in Eqs. (3.10)–(3.12).

We include the mixing between the states on the two halves of the Fermi surface, i.e., plane-wave states $|\vec{k} + \vec{Q}\rangle$ with $|\vec{k} - \vec{Q}\rangle$. This is accomplished through the use of nondegenerate perturbative corrections of first order in the wave functions and of second order in the energies. The new expression for $E_{\vec{k}}$ may then be written

$$E_{\vec{k}} = \frac{\hbar^2 Q^2}{2m} \left(\kappa^2 + w^2 + \frac{1}{4} - (w^2 + \alpha^2)^{1/2} - \frac{\alpha^2}{2(1 - |w|)} \right) . \qquad (3.14)$$

The corresponding wave function is

$$\Psi_{\vec{k}} = (1 + C_{\vec{k}}^2)^{-1/2}(A_{\vec{k}} e^{i\vec{k}\cdot\vec{r}} + B_{\vec{k}} e^{i(\vec{k}+\vec{Q})\cdot\vec{r}} + C_{\vec{k}} e^{i(\vec{k}-\vec{Q})\cdot\vec{r}}) , \quad k_z < 0 \qquad (3.15a)$$

$$\Psi_{\vec{k}} = (1 + C_{\vec{k}}^2)^{-1/2}(A_{\vec{k}}e^{i\vec{k}\cdot\vec{r}} + B_{\vec{k}}e^{i(\vec{k}-\vec{Q})\cdot\vec{r}}$$
$$+ C_{\vec{k}}e^{i(\vec{k}+\vec{Q})\cdot\vec{r}}), \quad k_z > 0 \quad (3.15b)$$

where $A_{\vec{k}} = \cos\varphi_{\vec{k}}$, $B_{\vec{k}} = -\sin\varphi_{\vec{k}}$, and

$$C_{\vec{k}} = \tfrac{1}{2}\alpha/(1 - |w|). \quad (3.15c)$$

The equation of critical contact is given by

$$E_{\vec{k}} = E_F = (\hbar^2 Q^2/2m)(\tfrac{1}{4} - \alpha - \tfrac{1}{2}\alpha^2). \quad (3.16)$$

Thus, the equation for the Fermi surface may be written as

$$\kappa = [(w^2 + \alpha^2)^{1/2} - \alpha - w^2 + \tfrac{1}{2}\alpha^2 |w|/(1 - |w|)]^{1/2}. \quad (3.17)$$

We obtain the appropriate value of Q by setting the volume within the Fermi surface for a given G equal to the volume of the free-electron sphere,

$$2\pi Q^3 \int_0^{1/2} \kappa^2 \, dw = \frac{4\pi}{3}k_F^3 = 4\pi n, \quad (3.18)$$

where n is the number of electrons per unit volume. From Eq. (3.17) we evaluate this integral and obtain the approximate expression for Q:

$$Q = 2k_F \left\{ 1 + \frac{\tilde{G}}{4} - \frac{\tilde{G}^2}{32}\left[\frac{\ln(16/\tilde{G}) + \tfrac{2}{3}\tilde{G}}{1 + \tfrac{1}{2}\tilde{G}}\right] \right\}, \quad (3.19)$$

where $\tilde{G} = G/E_F^0$. For this value of Q, the difference between the volume within the Fermi surface and that within the free-electron sphere is less than 0.05% for values of $\tilde{G}$ up to 0.5.

In Fig. 4, using Eq. (3.19), we plot the variation of Q from $2k_F$, $Q/2k_F - 1$, as a function of G/E_F^0. In addition, we plot α from Eq. (3.11b). Another consequence of the CDW with its lemon-shaped Fermi surface is to decrease the Fermi energy E_F below its free-electron value E_F^0. This variation, $1 - E_F/E_F^0$, is also plotted in Fig. 4. Note that Q deviates substantially from the linear approximation given by Eq. (3.13).
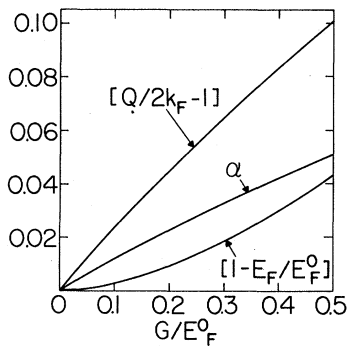

FIG. 4. Plots of the deviations of Q, α, and E_F from their free-electron values, or values at $G = 0$, vs G/E_F^0.
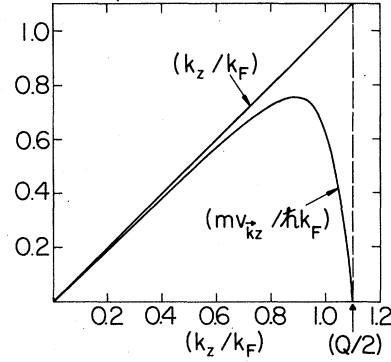

FIG. 5. Comparison of v_z with k_z as a function of k_z for $G/E_F^0 = 0.5$.

Another quantity important in following calculations is the velocity of electrons in the z direction along $\vec{Q}$. This is given by

$$v_z = \frac{\partial E_{\vec{k}}}{\partial k_z} = \frac{\hbar Q}{m}\left(w - \frac{w}{2(w^2 + \alpha^2)^{1/2}} - \frac{\alpha^2 w/|w|}{4(1 - |w|)^2}\right). \quad (3.20)$$

In Fig. 5, for $G/E_F^0 = 0.5$, we compare the plot of v_z with that of k_z as a function of k_z for $k_z > 0$. Note that at the conical point ($k_z = \tfrac{1}{2}Q$ or $w = 0$) the electron velocity nearly vanishes. This has important consequences, as will be discussed in Sec. IV.

An additional check on the validity of the preceding approximations, we calculate the volume by another method, which involves the electron velocity, to compare with that of the free-electron sphere.

$$4\pi n = \frac{4}{3}\pi k_F^3 = -\frac{1}{4\pi^3}\int v_{\vec{k}z}k_z \frac{\partial f_{\vec{k}}^0}{\partial E_{\vec{k}}} \, d^3k$$

$$= \pi Q^3 \int_0^{1/2} \hat{v}_z \hat{k}_z \, dw, \quad (3.21)$$

where $\hat{v}_z = (m/\hbar Q)v_z$ and $\hat{k}_z = k_z/Q$, and where $f_{\vec{k}}^0$ is the equilibrium distribution function of the electron gas. For Q given by Eq. (3.19), the equality of Eq. (3.21) is accurate to within 0.7% for $\tilde{G}$ values up to 0.5.

IV. MODEL SCATTERING POTENTIALS

Since electrons cannot scatter from a perfect lattice, a nonzero resistivity in a metal can arise only if irregularities occur in the lattice. At high temperatures phonons provide this disturbance and a temperature-dependent resistivity results. However, when the temperature approaches absolute zero, the effects of phonons become unimportant, and the remaining temperature-indepen-

dent resistivity, the residual resistivity, arises through the scattering of conduction electrons from stationary imperfections. If the potential produced by the presence of an impurity is sufficiently weak, the cross section for scattering can be determined within the Born approximation, requiring knowledge only of the Fourier transform of the impurity potential.

In this section we introduce the models for impurity-scattering potentials that will be used in succeeding sections, along with their Fourier transforms. In high-purity alkali metals impurities predominantly enter the crystal substitutionally. Thus, the potential from which electrons scatter is that of the impurity minus that of the missing lattice ion. For mathematical convenience, we will assume a Gaussian form for potentials of lattice and impurity ions, and for convenience in the discussion, we will refer to the host metal as potassium. A potassium ion in the lattice has a potential of the form

$$v_a(\vec{r}) = V_a e^{-r^2/\Gamma_a^2}, \qquad (4.1)$$

where $\Gamma_a = ar_s$, with r_s the Wigner-Seitz radius. The corresponding Fourier transform is

$$\tilde{v}_a(\vec{q}) = \int d^3r\, e^{-i\vec{q}\cdot\vec{r}} v_a(\vec{r})$$

$$= V_a \pi^{3/2} \Gamma_a^3 \exp(-\tfrac{1}{4}\Gamma_a^2 q^2). \qquad (4.2)$$

If the height V_b of the potential of the impurity ion is different from the height V_a of the potential of the K ion that it replaces, but the width is the same, then the scattering potential will be given by

$$v_1(\vec{r}) = V_1 e^{-r^2/\Gamma_a^2}, \qquad (4.3)$$

where $V_1 = V_b - V_a$. The Fourier transform $\tilde{v}_1(\vec{q})$ is the same form as Eq. (4.2). If, on the other hand, the width Γ_b of the impurity potential is different from the width Γ_a of the K ion potential, but the height is the same, then the scattering potential is

$$v_2(\vec{r}) = v_b(\vec{r}) - v_a(\vec{r}), \qquad (4.4)$$

where $v_b(\vec{r})$ is obtained from $v_a(\vec{r})$ by replacing Γ_a with Γ_b. The Fourier transform is given by

$$\tilde{v}_2(\vec{q}) = \tilde{v}_b(\vec{q}) - \tilde{v}_a(\vec{q}). \qquad (4.5)$$

The results of the combination of these two cases that might occur will not be considered here, since this would add unnecessary complications without providing additional insight.

In addition to the scattering potential of the impurity ion itself, an additional potential can arise due to a strain field created by the introduction of an impurity into the lattice.[18] The surrounding

ions adjust their positions in order to compensate for the misfit of the impurity in the lattice. The strain-field potential is given by the difference between the new positions of the K ions and their positions in the perfect lattice. For a substitutional impurity at the origin, we sum over all lattice points $\vec{L}$ except that of the impurity and write the potential as

$$v_s(\vec{r}) = \sum_{\vec{L} \neq 0} [(v_a(\vec{r} - \vec{L} - \vec{u}_{\vec{L}}) - v_a(\vec{r} - \vec{L})], \qquad (4.6)$$

where $\vec{u}_{\vec{L}}$ is the displacement vector of the ion at site $\vec{L}$. The Fourier transform is given by

$$\tilde{v}_s(\vec{q}) = \tilde{v}_a(\vec{q}) \sum_{\vec{L} \neq 0} e^{-i\vec{q}\cdot\vec{L}} (e^{-i\vec{q}\cdot\vec{u}_{\vec{L}}} - 1). \qquad (4.7)$$

For small displacements, we may expand the exponential involving $\vec{u}_{\vec{L}}$ and write approximately

$$\tilde{v}_s(\vec{q}) = \tilde{v}_a(\vec{q}) \sum_{\vec{L} \neq 0} (-i\vec{q}\cdot\vec{u}_{\vec{L}}) e^{-i\vec{q}\cdot\vec{L}}. \qquad (4.8)$$

We choose a form for $\vec{u}_{\vec{L}}$ appropriate to that of a spherical center of dilatation in an infinite elastic medium,[18,19]

$$\vec{u}_{\vec{L}} = g a_0^3 \vec{L}/L^3, \qquad (4.9)$$

where a_0 is the lattice constant of a bcc lattice and g is a dimensionless constant. We do not use a separate form for the nearest neighbors as for the case of interstitial impurities in Ref. 18 since here the nearest neighbors are approximately as distant from the impurity as the next-nearest neighbors in that case. With Eq. (4.9), Eq. (4.8) reduces to

$$\tilde{v}_s(\vec{q}) = \tilde{v}_a(\vec{q}) S(\vec{q}), \qquad (4.10a)$$

where

$$S(\vec{q}) = -i g a_0^3 \sum_{\vec{L} \neq 0} \frac{\vec{q}\cdot\vec{L}}{L^3} e^{-i\vec{q}\cdot\vec{L}}. \qquad (4.10b)$$

As we shall see in Sec. V, the calculation of the residual resistivity with Eq. (4.10) requires numerical calculation of a four-dimensional integral. The contribution from each term in the sum of Eq. (4.10b) contains many spikes, part of whose contribution is cancelled by higher-order terms. In addition, many sine functions must be computed at each point in the integrand. The integrations are thus difficult to perform and the rate of increase in the cost of computing contributions from each successive term far exceeds the slow rate of convergence of the sum. For this reason, we make a simplifying assumption, as was used in Ref. 18, that reduces necessary numerical integrations to three dimensions, reduces the number of sine functions in the integrand, and improves the con-

vergence of the sum. We assume that the N_s sth-nearest neighbors are smeared into a spherical shell of radius L_s, the sth-nearest-neighbor distance. This is accomplished by replacing the sum over the neighbors within a shell by an integral corresponding to an angular average and summing over the shells. This yields

$$S(\vec{q}) \cong -iga_0^3 \sum_s \frac{N_s}{4\pi L_s^3} \int qL_s \cos\theta\, e^{-iqL_s\cos\theta} d\Omega$$

$$= ga_0^3 \sum_s \frac{N_s}{L_s^3}\left(\cos(qL_s) - \frac{\sin(qL_s)}{qL_s}\right). \quad (4.11)$$

Since one can, in practice, sum over only a finite number s_f of shells, we compute the remainder to the sum by assuming that the atoms beyond the s_fth shell are spread into a continuum,

$$\sum_{s=s_f}^{\infty} \frac{\vec{q}\cdot\vec{L}}{L^3} e^{-i\vec{q}\cdot\vec{L}} = \frac{2}{a_0}\int_{r_0}^{\infty} L^2\, dL \int \frac{Lq\cos\theta}{L^3}$$

$$\times e^{-iqL\cos\theta}\, d\Omega$$

$$= \frac{-8\pi i}{a_0^3}\frac{\sin(qr_0)}{qr_0}, \quad (4.12)$$

where $r_0 = N_t^{1/3} r_s$ is the radius of a sphere equal to N_t atomic volumes, with

$$N_t = 1 + \sum_{s=1}^{s_f} N_s, \quad (4.13)$$

counting the atoms included in the shells plus the impurity. Combining Eqs. (4.11) and (4.12), we have

$$S(\vec{q}) \cong g\left[\sum_{s=1}^{s_f} N_s\left(\frac{a_0}{L_s}\right)^3\left(\cos(qL_s) - \frac{\sin(qL_s)}{qL_s}\right)\right.$$

$$\left. - 8\pi\frac{\sin(qr_0)}{qr_0}\right]. \quad (4.14)$$

We have computed the necessary integrals for the computation of the residual resistivity and have summed shells out to 17th-nearest neighbors ($s_f = 17$). Good convergence occurs after the inclusion of $s_f = 14$.

Since the total impurity potential arises from a combination of a central-ion potential, $v_1(\vec{r})$ or $v_2(\vec{r})$, and the strain potential $v_s(\vec{r})$, we define two additional potentials that include this. We assume that the central-ion potential contributes a fraction $1 - x$ and the strain potential a fraction x to the total potential. In order to simplify this portion of the calculation (and reduce the cost of the integrations), we approximate $S(\vec{q})$ in Eq. (4.14) with the continuum term $s_f = 0$, choosing r_0 so that the same resitivities are obtained as with $s_f = 14$. The Fourier transform of the result-

ing "interference" potential involving $v_1(\vec{r})$ is given by

$$\tilde{v}_{\text{int}}^{(1)}(\vec{q}) = g(V_a/V_1)\beta(1-x)\tilde{v}_1(\vec{q}) + x\tilde{v}_s(\vec{q}) \quad (4.15a)$$

$$= g\tilde{v}_a(\vec{q})[\beta(1-x) - 8\pi x(\sin qr_0/qr_0)], \quad (4.15b)$$

where β is chosen for each Γ_a such that the resistivity in the absence of a CDW is the same for $x = 0$ as for $x = 1$. The Fourier transform of the corresponding potential involving $v_2(\vec{r})$ is

$$\tilde{v}_{\text{int}}^{(2)}(\vec{q}) = g\beta(1-x)\tilde{v}_2(\vec{q}) + x\tilde{v}_s(\vec{q}) \quad (4.16a)$$

$$= g\left[\beta(1-x)\tilde{v}_b(\vec{q}) - \tilde{v}_a(\vec{q})\right.$$

$$\left. \times\left(\beta(1-x) + 8\pi x\frac{\sin qr_0}{qr_0}\right)\right], \quad (4.16b)$$

where again β is chosen to make resistivities for $x = 0$ and $x = 1$ equal. In both cases [Eqs. (4.15) and (4.16)], β positive corresponds to g positive (outward displacements of neighbors about the impurity) and β negative to g negative (inward displacements).

We note that the Fourier transforms of the above potentials are effective pseudopotentials for the impurities. Values of $\Gamma \sim r_s$ represent the widths of typical pseudopotential calculations in K.[20] Values within this range cause $\tilde{v}(\vec{q})$ for each of the models presented here to be sharply peaked about $\vec{q} = 0$. This has important consequences in the effects of a CDW on the residual resistivity, which will be explained in Sec. V.

V. RESIDUAL-RESISTIVITY CALCULATION

When an electric field $\vec{\mathscr{E}}$ is applied to a metal, the electrons are accelerated in such a way that their equilibrium distribution function $f_{\vec{k}}^0$ is shifted at a constant rate in $\vec{k}$ space, with the distribution function $f_{\vec{k}}$ after a time (Δt) given by[21]

$$f(\vec{k}) = f_0(\vec{k} - \vec{\delta}), \quad (5.1a)$$

where

$$\vec{\delta} = -e\vec{\mathscr{E}}(\Delta t)/\hbar. \quad (5.1b)$$

For $\vec{\mathscr{E}}$ in the μ direction, we may write

$$f(\vec{k}) \approx f_0(\vec{k}) - \delta_\mu\frac{\partial f_0(\vec{k})}{\partial k_\mu} = f_{\vec{k}}^0 - \delta_\mu v_{\vec{k}\mu}\frac{\partial f_{\vec{k}}^0}{\partial E_{\vec{k}}}, \quad (5.2)$$

where $v_{\vec{k}\mu} = \partial E_{\vec{k}}/\partial k_\mu$ is the velocity of electrons in the state $|\Psi_{\vec{k}}\rangle$ in the μ direction. The current density in the metal is then

$$\vec{J} = e\vec{P}/m, \quad (5.3a)$$

with

$$\vec{P} = \int \frac{d^3k}{4\pi^3} m v_{\vec{k}} f_{\vec{k}} , \tag{5.3b}$$

so that $\vec{J}$ is proportional to the total momentum $\vec{P}$ of the electrons. For the shifted Fermi distribution of Eqs. (5.1) and (5.2), the current density in the μ direction may be written as

$$J_\mu = e\delta_\nu \int \frac{d^3k}{4\pi^3} v_{\vec{k}\mu} v_{\vec{k}\nu} \frac{\partial f_{\vec{k}}^0}{\partial E_{\vec{k}}}$$

$$= c\delta_\mu \int \frac{d^3k}{4\pi^3} v_{\vec{k}\mu}^2 \frac{\partial f_{\vec{k}}^0}{\partial E_{\vec{k}}} . \tag{5.4}$$

For $\mu \neq \nu$, the integral above clearly vanishes for μ, ν Cartesian coordinates and the principal axes in the electron gas described in Sec. III. The current is thus only along $\vec{\mathcal{E}}$.

In a perfect crystal, this acceleration due to an electric field would take place indefinitely, leading to an infinite current density. However, any real metal contains impurities, so that electrons suffer collisions and the system reaches a steady state. At finite temperatures, electrons also interact with phonons, but here we consider only the limit of zero temperature. In the steady state the distribution function is displaced by an amount $\vec{\delta}$, where a relaxation time τ replaces (Δt) in Eq. (5.1b). A determination of the magnitude of $\vec{\delta}$ leads one to an expression for the resistivity by employing Eq. (5.4).

The actual distribution function of an electron gas in the steady-state situation described above is not exactly that of a rigidly shifted equilibrium distribution function, but must be obtained from a solution of the equation that equates the rate of change of $f_{\vec{k}}$ due to $\vec{\mathcal{E}}$ with that due to collisions, the linearized Boltzmann transport equation,[22]

$$-e(\vec{v}_{\vec{k}} \cdot \vec{\mathcal{E}}) \frac{\partial f_{\vec{k}}^0}{\partial E_{\vec{k}}} = \int \frac{d^3k'}{4\pi^3} [(f_{\vec{k}} - f_{\vec{k}}^0)$$

$$- (f_{\vec{k}'} - f_{\vec{k}'}^0)] \mathcal{Q}_{\vec{k}}^{\vec{k}'} , \tag{5.5}$$

where $\mathcal{Q}_{\vec{k}}^{\vec{k}'}$ is the golden-rule transition rate, describing the elastic scattering of electrons from a potential $\mathcal{V}_{tot}(\vec{r})$ of all the impurities in the crystal.

$$\mathcal{Q}_{\vec{k}}^{\vec{k}'} = (2\pi/\hbar) |M_{\vec{k}', \vec{k}}|^2 \delta(E_{\vec{k}} - E_{\vec{k}'}) \tag{5.6a}$$

with

$$M_{\vec{k}', \vec{k}} = \langle \Psi_{\vec{k}'} | \mathcal{V}_{tot}(\vec{r}) | \Psi_{\vec{k}} \rangle . \tag{5.6b}$$

For practical purposes, however, it suffices to assume the form (5.2) for $f_{\vec{k}}$ and to impose a slightly weaker condition than Eq. (5.5), that is, that the rate of change of the total momentum of the electrons balance in the steady state. Since the rate of change of $\vec{P}$ is given by

$$\frac{d\vec{P}}{dt} = \int \frac{d^3k}{4\pi^3} m \vec{v}_{\vec{k}} \frac{\partial f_{\vec{k}}}{\partial t} , \tag{5.7}$$

the required condition is obtained by multiplying both sides of Eq. (5.5) by $m\vec{v}_{\vec{k}}$ and integrating over $d^3k/4\pi^3$ to yield

$$-em\mathcal{E}_\mu \int \frac{d^3k}{4\pi^3} v_{\vec{k}\mu}^2 \frac{\partial f_{\vec{k}}^0}{\partial E_{\vec{k}}}$$

$$= \frac{-m\delta_\mu}{2} \int \frac{d^3k}{4\pi^3} \int \frac{d^3k'}{4\pi^3} (v_{\vec{k}\mu} - v_{\vec{k}'\mu})^2 \frac{\partial f_{\vec{k}}^0}{\partial E_{\vec{k}}} \mathcal{Q}_{\vec{k}}^{\vec{k}'} , \tag{5.8}$$

which may be solved trivially for δ_μ. The resistivity is then obtained by substituting δ_μ into Eq. (5.4).

The procedure outlined here is equivalent to employing the variational principle to determine the resistivity tensor,[23]

$$\rho_{\mu\mu} = -\frac{1}{2} \int d^3k \int d^3k' (\Phi_{\vec{k}\mu} - \Phi_{\vec{k}'\mu})^2 \mathcal{Q}_{\vec{k}}^{\vec{k}'} \frac{\partial f_{\vec{k}}^0}{\partial E_{\vec{k}}} \bigg/ \left| \int d^3k \, e v_{\vec{k}\mu} \Phi_{\vec{k}\mu} \left(\frac{\partial f_{\vec{k}}^0}{\partial E_{\vec{k}}} \right) \right|^2 , \tag{5.9}$$

with a trial function given by $\Phi_{\vec{k}\mu} = v_{\vec{k}\mu}$. This variational expression provides an upper bound on the resistivity, so that the actual resistivity must be less than or equal to that calculated using any given trial function in Eq. (5.9).

When the conduction electrons are in a CDW ground state, as described in Sec. III, the residual resistivity is enhanced more along $\vec{Q}$ than it is perpendicular to $\vec{Q}$, resulting in an anisotropy. The principal factor contributing to this effect is $|M_{\vec{k}', \vec{k}}|^2$, the square of the matrix element in Eq. (5.6b), which appears in the golden-rule transition rate in Eq. (5.6a). The total potential $\mathcal{V}_{tot}(\vec{r})$, due to all the N_I impurities in the crystal, is the sum over all the single impurity potentials $\mathcal{V}(\vec{r})$ located at sites $\vec{R}_i$,

$$\mathcal{V}_{tot}(\vec{r}) = \sum_{i=1}^{N_I} \mathcal{V}(\vec{r} - \vec{R}_i) , \tag{5.10}$$

where $v(\vec{r})$ represents one of the model potentials described in Sec. IV. For $k_z > 0$, $k_z' > 0$, the matrix element becomes

$$M_{\vec{k}',\vec{k}} = [(1 + C_{\vec{k}}^2)(1 + C_{\vec{k}'}^2)]^{-1/2} \sum_{i=1}^{N_I} [(A_{\vec{k}} A_{\vec{k}'} + B_{\vec{k}} B_{\vec{k}'} + C_{\vec{k}} C_{\vec{k}'}) e^{i(\vec{k}-\vec{k}')\cdot\vec{R}_i} \tilde{v}(\vec{k}-\vec{k}') + (A_{\vec{k}} B_{\vec{k}'} + C_{\vec{k}} A_{\vec{k}'}) e^{i(\vec{k}-\vec{k}'+\vec{Q})\cdot\vec{R}_i}$$

$$\times \tilde{v}(\vec{k}-\vec{k}'+\vec{Q}) + (A_{\vec{k}} C_{\vec{k}'} + B_{\vec{k}} A_{\vec{k}'}) e^{i(\vec{k}-\vec{k}'-\vec{Q})\cdot\vec{R}_i} \tilde{v}(\vec{k}-\vec{k}'-\vec{Q}) + (B_{\vec{k}} C_{\vec{k}'}) e^{i(\vec{k}-\vec{k}'-2\vec{Q})\cdot\vec{R}_i}$$

$$\times \tilde{v}(\vec{k}-\vec{k}'-2\vec{Q}) + (C_{\vec{k}} B_{\vec{k}'}) e^{i(\vec{k}-\vec{k}'+2\vec{Q})\cdot\vec{R}_i} \tilde{v}(\vec{k}-\vec{k}'+2\vec{Q})] . \tag{5.11}$$

If the impurities are distributed at random,[24] the cross terms in $|M_{\vec{k}',\vec{k}}|^2$ cancel, and the result is proportional to $\hat{N}_I$, the number of impurities per unit volume. For $k_z > 0$, $k_z' > 0$,

$$|M_{\vec{k}',\vec{k}}|^2 = \hat{N}_I [(1 + C_{\vec{k}}^2)(1 + C_{\vec{k}'}^2)]^{-1} [(A_{\vec{k}} A_{\vec{k}'} + B_{\vec{k}} B_{\vec{k}'} + C_{\vec{k}} C_{\vec{k}'})^2 \tilde{v}^2(\vec{k}-\vec{k}') + (A_{\vec{k}} B_{\vec{k}'} + C_{\vec{k}} A_{\vec{k}'})^2 \tilde{v}^2(\vec{k}-\vec{k}'+\vec{Q})$$

$$+ (A_{\vec{k}} C_{\vec{k}'} + B_{\vec{k}} A_{\vec{k}'})^2 \tilde{v}^2(\vec{k}-\vec{k}'-\vec{Q}) + (B_{\vec{k}} C_{\vec{k}'})^2 \tilde{v}^2(\vec{k}-\vec{k}'-2\vec{Q})$$

$$+ (C_{\vec{k}} B_{\vec{k}'})^2 \tilde{v}^2(\vec{k}-\vec{k}'+2\vec{Q})] . \tag{5.12a}$$

Similarly, for $k_z > 0$, $k_z' < 0$,

$$|M_{\vec{k}',\vec{k}}|^2 = \hat{N}_I [(1 + C_{\vec{k}}^2)(1 + C_{\vec{k}'}^2)]^{-1} [(A_{\vec{k}} A_{\vec{k}'} + B_{\vec{k}} C_{\vec{k}'} + C_{\vec{k}} B_{\vec{k}'})^2 \tilde{v}^2(\vec{k}-\vec{k}') + (A_{\vec{k}} B_{\vec{k}'} + B_{\vec{k}} A_{\vec{k}'})^2 \tilde{v}^2(\vec{k}-\vec{k}'-\vec{Q})$$

$$+ (A_{\vec{k}} C_{\vec{k}'} + C_{\vec{k}} A_{\vec{k}'})^2 \tilde{v}^2(\vec{k}-\vec{k}'+\vec{Q}) + (B_{\vec{k}} B_{\vec{k}'})^2 \tilde{v}^2(\vec{k}-\vec{k}-2\vec{Q})$$

$$+ (C_{\vec{k}} C_{\vec{k}'})^2 \tilde{v}^2(\vec{k}-\vec{k}'+2\vec{Q})] . \tag{5.12b}$$

The expressions for $k_z < 0$, $k_z' < 0$, and for $k_z < 0$, $k_z' > 0$ may be obtained by replacing $\vec{Q}$ by $-\vec{Q}$ in Eqs. (5.12a) and (5.12b), respectively.

Examination of Eqs. (5.12), aided by Fig. 6, reveals the source of the resistivity anisotropy. Let Θ be the scattering angle, or the angle between $\vec{k}$ and $\vec{k}'$. The factor $(v_{\vec{k}\mu} - v_{\vec{k}\mu})^2$ on the right-hand side of Eq. (5.8), which is proportional to $(1 - \cos\Theta)$ for a spherical Fermi surface (no CDW), weights 180° scattering heavily and small-angle scattering lightly. As explained in Sec. IV, the Fourier transform of the impurity scattering
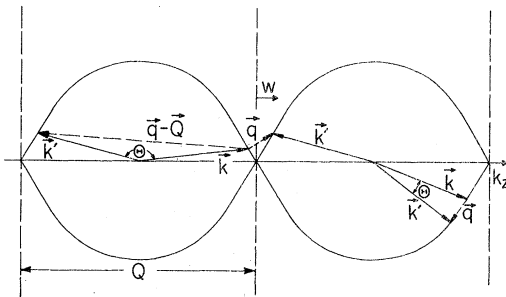

FIG. 6. Diagram illustrating the umklapp scattering (left portion of figure) vs the normal scattering (right portion) when the conservation rule of Eq. (5.13) is taken into account. The distortion of the conical-point regions is exaggerated for emphasis.

potential $\tilde{v}(\vec{q})$ is sharply peaked about $\vec{q} = 0$. In the absence of a CDW ($A_{\vec{k}} = 1$, $B_{\vec{k}} = C_{\vec{k}} = 0$), with $\vec{q} = \vec{k}' - \vec{k}$, the scattering cross section thus weights small $\vec{q}$'s the most, which in this case is the same as small angles Θ, as is shown in the right half of Fig. 6. No preference exists in any particular direction, so the scattering of electrons, and thus the resistivity, is isotropic. In the presence of a CDW, however, the mixing of plane waves, which is responsible for the form of the wave functions $\Psi_{\vec{k}}$, creates a totally different situation. In this case, small-$\vec{q}$ Fourier components of the potential may scatter electrons according to the conservation rule

$$\vec{k}' = \vec{k} + \vec{q} \pm \vec{Q} . \tag{5.13}$$

The result is shown in Fig. 6 on the left, within the reduced-zone scheme, for a wave-vector transfer $\vec{k}$ to $\vec{k}'$ from the conical-point region on one side of the Fermi surface to the other conical-point region on the opposite side. Here Θ is nearly 180°, so that this transition is favored by the weighting factor. Therefore, the scattering along the direction of $\vec{Q}$ (the z direction) is greatly enhanced. This may be viewed alternatively in the repeated zone scheme, as shown in Fig. 6. The wave-vector transfer $\vec{q}$ between $\vec{k}$ and $\vec{k}'$ scatters an electron from a state on the Fermi surface in one zone to another state in the next, because in the presence of a CDW this distance is very short in the conical-point region. Since only transitions

that are parallel to $\vec{\mathcal{E}}$ contribute to the resistivity, this umklapp scattering does not affect the resistivity perpendicular to the CDW (perpendicular to $\vec{Q}$).

While the factor $(v_{\vec{k}z} - v_{\vec{k}'z})^2$ in the calculation of the component ρ_{zz} of the resistivity tensor enhances umklapp scattering, $v_{\vec{k}z}$ vanishes at the conical point, or at $k_z = \frac{1}{2}Q$, as shown in Fig. 5. This means that only umklapp transitions between states near the conical points contribute, not transitions between states at the points themselves.

The effect can be seen explicitly as a necessary consequence of Eqs. (5.12). For $k_z > 0$, $k_z' > 0$ or $k_z < 0$, $k_z' < 0$, the scattering occurs only within one half of the Fermi surface and does not involve umklapp scattering. However, for $k_z > 0$, $k_z' < 0$ or $k_z < 0$, $k_z' > 0$, the CDW-umklapp effect becomes important. In Eq. (5.12b), the term involving $\tilde{U}^2(\vec{k} - \vec{k}' - \vec{Q})$ is sharply peaked about $\vec{k} - \vec{k}' = \vec{Q}$, and weights the type of transition described by Eq. (5.13). In addition, the coefficient $(A_{\vec{k}}B_{\vec{k}'} + A_{\vec{k}'}B_{\vec{k}})^2$ in the region near $k_z \sim \frac{1}{2}Q$ is as large as the coefficient of the first term and larger than the

coefficients of the others. For $k_z < 0$, $k_z' > 0$, the corresponding term involves the same coefficient with $\tilde{U}^2(\vec{k} - \vec{k}' + \vec{Q})$. Note that if $\upsilon(\vec{r})$ were a delta function, $\tilde{\upsilon}(\vec{q})$ would be a constant and the CDW-umklapp transitions would no longer be enhanced. Clearly, the resistivity anisotropy depends on the localization of $\tilde{\upsilon}(\vec{q})$ about $\vec{q} = 0$. The more sharply peaked $\tilde{\upsilon}(\vec{q})$ is, the greater will be the anisotropy. This means that the more extended the potential is in real space, the greater will be the anisotropy.

We now proceed with the calculation of the residual resistivity. In order to perform the integrations indicated in Eq. (5.8), we invoke the zero-temperature equality $\partial f_{\vec{k}}^0/\partial E_{\vec{k}} = -\delta(E_{\vec{k}} - E_F)$ and transform integrations over d^3k to integrations over energy and the dimensionless cylindrical coordinates of Sec. III,

$$d^3k = (m/\hbar^2)Q\,d\theta\,dw\,dE_{\vec{k}}, \qquad (5.14)$$

where θ is the polar angle. In addition, we define $\psi = \theta - \theta'$ and $\psi = \frac{1}{2}(\theta + \theta')$, so that $d\theta\,d\theta' = d\psi\,d\psi'$. As an illustration, we consider the first model potential of Sec. IV, given by Eq. (4.3). We define

$$T_\mu = \frac{Q}{k_F}\frac{(\Gamma_a k_F)^6}{32\pi^2}\int_{-1/2}^{1/2}dw\int_{-1/2}^{1/2}dw'\int_0^{2\pi}d\psi\int_0^{2\pi}d\psi'(v_{\vec{k}\mu} - v_{\vec{k}'\mu})^2|\hat{M}_{\vec{k}',\vec{k}}|^2, \qquad (5.15a)$$

where

$$|M_{\vec{k}',\vec{k}}|^2 = (\bar{N}_I V_1^2 \pi^3 \Gamma_a^6)|\hat{M}_{\vec{k}',\vec{k}}|^2, \qquad (5.15b)$$

and

$$F = 3\left(\frac{Q}{k_F}\right)^3\int_0^{1/2} v_{\vec{k}\mu}^2\,dw. \qquad (5.15c)$$

Here, $\bar{N}_I = \hat{N}_I/n$ is the fractional number of impurities in the metal. If we define

$$\delta_\mu = -e\mathcal{E}_\mu\tau_\mu/\hbar, \qquad (5.16a)$$

then

$$\rho_{\mu\nu} = (m/ne^2\tau_\mu)\delta_{\mu\nu}, \qquad (5.16b)$$

where $\delta_{\mu\nu}$ is the Kronecker δ. Combining Eqs.

(5.4), (5.8), (5.15), and (5.16), we have

$$\frac{1}{\tau_z} = \bar{N}_I\frac{V_1^2}{\hbar E_F^0}\frac{T_z}{|F|^2}, \quad \frac{1}{\tau_x} = \frac{1}{\tau_y} = \bar{N}_I\frac{V_1^2}{\hbar E_F^0}T_x, \qquad (5.17)$$

so that the resistivity ratio is given by

$$\gamma = \frac{\rho_{zz}}{\rho_{xx}} = \frac{1}{|F|^2}\frac{T_z}{T_x}. \qquad (5.18)$$

Note that γ does not depend on the overall strength of the scattering potential or on the number of impurities present.

Equation (5.15) may be written explicitly for the x and z directions, with the substitutions $v_{\vec{k}x} = \hbar k_x/m$ and $v_{\vec{k}z} = (\hbar Q/m)\hat{v}_{\vec{k}z}$ and an integration over ψ', as

$$T_z = \left(\frac{Q}{k_F}\right)^4\frac{(\Gamma_a k_F)^6}{16\pi}\int_{-1/2}^{1/2}dw\int_{-1/2}^{1/2}dw'\int_0^{2\pi}d\psi(\hat{v}_{\vec{k}z} - \hat{v}_{\vec{k}'z})^2|\hat{M}_{\vec{k}',\vec{k}}|^2, \qquad (5.19a)$$

$$T_x = \left(\frac{Q}{k_F}\right)^4 \frac{(\Gamma_a k_F)^6}{16\pi} \int_{-1/2}^{1/2} dw \int_{-1/2}^{1/2} dw' \int_0^{2\pi} d\psi [(\kappa^2 + \kappa'^2) - 2\kappa\kappa' \cos\psi] |\hat{M}_{\vec{k}',\vec{k}}|^2 , \tag{5.19b}$$

where κ is given by Eq. (3.17) of Sec. III. The factor $|\hat{M}_{\vec{k}',\vec{k}}|^2$ does not depend on ψ' and the ψ dependence can be factored out of all the terms in Eqs. (5.12), so that we may define

$$|\hat{M}_{\vec{k}',\vec{k}}|^2 = \exp\{-\tfrac{1}{2}\Gamma_a^2 Q^2 [(\kappa^2 + \kappa'^2) - 2\kappa\kappa' \cos\psi]\} |\bar{M}(k_z', k_z)|^2 . \tag{5.20}$$

Following integration over ψ, we have

$$T_z = \left(\frac{Q}{k_F}\right)^4 \frac{(\Gamma_a k_F)^6}{8} \int_{-1/2}^{1/2} dw \int_{-1/2}^{1/2} dw' (\hat{v}_{\vec{k}z} - \hat{v}_{\vec{k}'z})^2 I_0(\Gamma_a^2 Q^2 \kappa\kappa') |\bar{M}(k_z', k_z)|^2 , \tag{5.21a}$$

$$T_x = \left(\frac{Q}{k_F}\right)^4 \frac{(\Gamma_a k_F)^6}{8} \int_{-1/2}^{1/2} dw \int_{-1/2}^{1/2} dw' [\tfrac{1}{2}(\kappa^2 + \kappa'^2) I_0(\Gamma_a^2 Q^2 \kappa\kappa') - \kappa\kappa' I_1(\Gamma_a^2 Q^2 \kappa\kappa')] |\bar{M}(k_z', k_z)|^2 , \tag{5.21b}$$

where $I_0(z)$ and $I_1(z)$ are modified Bessel functions of the first kind of orders zero and one, respectively. These two-dimensional integrals must be carried out numerically for $G \neq 0$. However, for the case $G = 0$, $T_x = T_z$, $F = 1$, and the solution assumes the simple form, where $\tau_0 = \tau_x = \tau_y = \tau_z$:

$$\frac{1}{\tau_0} = \frac{\bar{N}_I}{6} \frac{V_1^2}{\hbar E_F^0} (\Gamma_a k_F)^2 (\Gamma k_F)^2 [(1 - e^{-2(\Gamma k_F)^2})$$
$$- 2(\Gamma_a k_F)^2 e^{-2(\Gamma k_F)^2}] . \tag{5.22}$$

If we let $\bar{V}_1 = (\Gamma_a k_F)^3 \pi^{3/2} V_1$ and constrain $\bar{V}_1$ to remain finite as $\Gamma_a \to 0$, then $v_1(\vec{r}) \to (\bar{V}_1/k_F^3)\delta(\vec{r})$ and τ_0 reduces to the form

$$\frac{1}{\tau_0} \to \frac{\bar{N}_I}{3\pi^3} \frac{\bar{V}_1^2}{\hbar E_F^0} . \tag{5.23}$$

In order for τ_0 to be that of sample K-10 of Holroyd and Datars (Fig. 1), $\tau \sim 1.4 \times 10^{-10}$ sec, with $\bar{N}_I = 10^{-5}$ from the reported purity, V_1 must be on the order of $\tfrac{1}{2}$ eV. This is determined by assuming Eq. (5.22) with $\Gamma_a \sim r_s$. This value is consistent with those of typical pseudopotential form factors.[20]

In the evaluation of the resistivity with $\tilde{v}_2(\vec{q})$, one obtains three terms, each of which is of the form of $\tilde{v}_1(\vec{q})$, and the analysis proceeds as above. For $\tilde{v}_s(\vec{q})$ an additional complication arises. Assuming the forms given in Eqs. (4.10) and (4.14), the steps through Eqs. (5.19) are unchanged. However, Eq. (5.20) no longer applies, since the additional factor of $S(\vec{q})$ enters each of the terms in Eqs. (5.12), and it is impossible to factor out the dependence on ψ or to perform the ψ integration analytically. Therefore, for this case, three-dimensional numerical integration is needed.

VI. NUMERICAL RESULTS

Before displaying the results of numerical calculations, we first appeal to experiments for an estimate of the range of values of G/E_F^0 appropriate to K. The CDW model has been successful in the explanations of the Mayer–El Naby optical anomaly[25] and the splitting of the conduction-electron-spin-resonance (CESR) lines.[26] The intense optical absorption with a threshold of 0.6 eV fixed the value of G/E_F^0 at about 0.29, assuming the free-electron mass. This same value produced a quantitative agreement with the CESR data. A
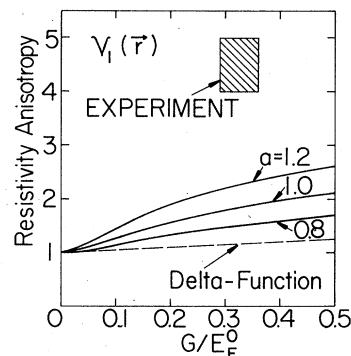
FIG. 7. Theoretical predictions for the resistivity anisotropy vs normalized CDW gap G/E_F^0 using the central-ion potential $v_1(\vec{r})$ from Eq. (4.3) of the text, for three values of a, where $\Gamma_a = a r_s$. Also shown is the anisotropy expected for a δ-function potential. The shaded rectangle represents the range of values determined by experiments.

maximum value for G/E_F^0 can be obtained by assuming that $E_F^0 = \hbar^2 k_F^2/2m^*$, where $m^* \approx 1.2m$, the measured cyclotron mass,[27] replaces m. This yields $G/E_F^0 \approx 0.36$. Thus, in Fig. 7 we indicate this range of values, along with the experimental values for the resistivity anisotropy from the torque anisotropy of Figs. 1 and 2, with a shaded rectangle. For K, G/E_F^0 lies between 0.29 and 0.36 and the resistivity anisotropy lies between 4 and 5 at 4 K. For comparison, we also show this shaded rectangle of experimental values in Figs. 8, 9, and 11. Clearly, for other alkali metals, a different set of values would be relevant.

We now show the theoretical predictions for the resistivity as a function of G/E_F^0 if one uses the various model scattering potentials described in Sec. IV and one calculates the resistivity in the manner described in Sec. V. The first case, shown in Fig. 7, is that for which the first central-ion potential $\upsilon_1(\vec{r})$ from Eq. (4.3), is used. We assume that the width Γ_a of the potential is comparable to the Wigner-Seitz radius r_s. In order to show the dependence of the results on this parameter, we let $\Gamma_a = ar_s$ and calculate the anisotropy with the values $a = 0.8, 1.0, 1.2$. Note that the larger Γ_a is, the greater is the spread of the potential in real space, but the more peaked is its Fourier transform in $\vec{q}$ space. If we allow the potential to go to the limit of a δ function, its Fourier transform is a constant, as discussed in Sec. V. In order to emphasize the importance of a sharply peaked Fourier transform for the enhancement of umklapp scattering, and eventually for a large resistivity anisotropy, we also plot in Fig. 7 the results of using a δ-function potential. It is clear that the sharp peaking of the Fourier transform about $\vec{q} = 0$ enhances the anisotropy and if no peaking occurs, the anisotropy is very small. The small effect that does occur for the δ-function potential is a consequence of the distorted shape of the Fermi surface. (See Figs. 3 and 6.) The elongated shape also produces a slight enhancement of the resistivity perpendicular to the CDW, since it decreases the distance for momentum transfer along that direction. This effect actually suppresses the anisotropy and has been included in these calculations.

The results using the second central-ion potential $\upsilon_2(\vec{r})$ of Eq. (4.4), are shown in Fig. 8. The width of the K ion is given by $\Gamma_a = ar_s$ and the width of the impurity ion by $\Gamma_b = br_s$. Since the potential appears squared in the calculations, the roles of these two could equally be reversed. Since this potential is formed by subtracting two Gaussians of the same heights but different widths, in real space the potential vanishes at the origin, so that $\upsilon_2(\vec{r})$ is more extended than either $\upsilon_a(\vec{r})$ or $\upsilon_b(\vec{r})$. Consequently, $\tilde{\upsilon}_2(\vec{q})$ is more localized about $\vec{q} = 0$
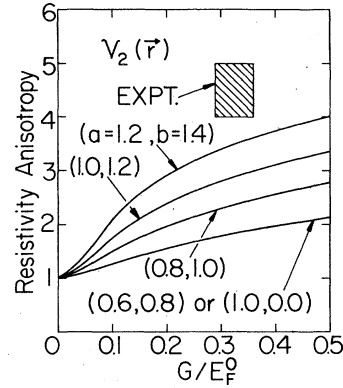

FIG. 8. Resistivity anisotropy vs G/E_F^0 using the central-ion potential $\upsilon_2(\vec{r})$ from Eq. (4.4), for four sets of values (a,b), where $\Gamma_a = ar_s$ and $\Gamma_b = br_s$. Note that the lowest curve is identical to that for $a = 1.0$ in Fig. 7.

than either $\tilde{\upsilon}_a(\vec{q})$ or $\tilde{\upsilon}_b(\vec{q})$. Its shape is nearly that of a Gaussian with a width Γ smaller than Γ_a or Γ_b. Thus this potential produces larger anisotropies than $\upsilon_1(\vec{r})$, as can be seen from Fig. 8. For instance, the lowest curve $(a, b) = (0.6, 0.8)$, is identical to the curve for $a = 1.0$ in Fig. 7. The difference between the widths of the Fourier transforms $\tilde{\upsilon}_a(\vec{q})$ and $\tilde{\upsilon}_b(\vec{q})$ can be represented by the quantity $a - b$. The anisotropy varies only slightly as this quantity is varied, as long as the average $\frac{1}{2}(a + b)$ remains constant. That is, the anisotropy produced by scattering from $\upsilon_2(\vec{r})$ is principally a function of $\frac{1}{2}(a + b)$.

In Figs. 7 and 8, we have used the value $\Gamma_a = 1.2r_s$ as the largest acceptable value for the width of the potential of a K ion in the lattice. This value was obtained by assuming that the magnitude of $\upsilon_a(\vec{r})$ at a distance r_s from the origin must be less than or equal to half its value at the origin. This implies that $a \lesssim 1/\sqrt{\ln 2} \approx 1.2$. A larger value would result in peaks in the positive background potential halfway between atoms. Values close to this represent a situation that most clearly resembles the jellium model of a uniform positive background. Of course, if one takes into account the actual bcc lattice of K, this maximum value of a should be slightly smaller.

We now turn to the results for the residual resistivity anisotropy for scattering of the electrons only from the strain field created by the presence of the impurity, shown in Fig. 9. We have used the potential $\upsilon_s(\vec{r})$ from Eq. (4.6), with the subsequent approximations for $\tilde{\upsilon}_s(\vec{q})$ in Eqs. (4.7)–(4.14). As discussed above, we use $a = 1.2$ as the maximum value of the width of the K-ion potential. In addition, we include the two other values $a = 0.8, 1.0$, as before. Since the strain field begins at the
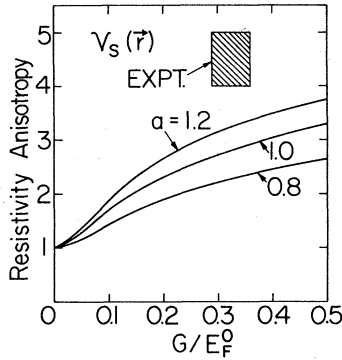
FIG. 9. Resistivity anisotropy vs G/E_F^0 using the strain-field potential $\mathcal{V}_s(\vec{r})$ from Eqs. (4.6), (4.10), and (4.14) of the text for three values of a.

FIG. 11. Maximum and minimum values for the resistivity anisotropy vs G/E_F^0 using the potential $\mathcal{V}_{int}^{(1)}(\vec{r})$, determined from Fig. 10 and similar plots, for three values of a. Also shown is the prediction from the standard "textbook model," for which the electron density is uniform throughout the metal (no CDW).

nearest-neighbor distance from the impurity and extends even farther, the Fourier transform $\tilde{v}_s(\vec{q})$ is more sharply peaked than $\tilde{v}_a(\vec{q})$ and thus produces a large anisotropy, considerably larger than that for $\tilde{v}_1(\vec{q})$ in Fig. 7.

Combining the scattering from the strain-field potential with either of the central-ion potentials can either increase or decrease the anisotropy, depending on the relative strengths of the potentials, which is determined by the parameter x in the expressions in Eqs. (4.15) and (4.16). The effects of combining the strain-field potential $\mathcal{v}_s(\vec{r})$ with the central-ion potential $\mathcal{v}_1(\vec{r})$, resulting in $\mathcal{v}_{int}^{(1)}(\vec{r})$ is illustrated in Fig. 10, for $G/E_F^0 = 0.35$ and $a = 1.0$. When $\beta < 0$, or for contraction of the lattice about the impurity, the anisotropy reaches a minimum when $x \approx 0.4$ and a maximum when $x \approx 0.65$. The value of the resistivity (in arbitrary units) for $G = 0$ is also shown. For this case, it is clear that the two potentials nearly cancel one another at $x = 0.5$. The minimum occurs when $\tilde{v}_{int}^{(1)}(\vec{q})$ achieves a cancellation near $\vec{q} = 0$, making the function more extended. Similarly, the maximum occurs when the cancellation occurs in the
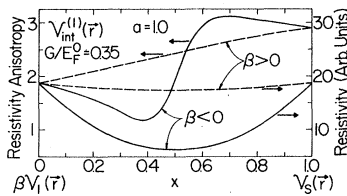
tails of the potentials, resulting in a more sharply peaked function about $\vec{q} = 0$. The results for $\beta > 0$ are also shown. For this case, since $\tilde{v}_1(\vec{q})$ and $\tilde{v}_s(\vec{q})$ add, no cancellation occurs, and the anisotropy varies nearly linearly with x.

Results for the maximum and minimum in Fig. 10 and similar plots is shown as a function of G/E_F^0 for three values of a in Fig. 11. The maximum anisotropies are larger than the curves in Figs. 7 and 9, and the highest curve, for $a = 1.2$, predicts anisotropies nearly as large as have been seen experimentally.

Finally, in Fig. 12, we show the dependence on x of the resistivity anisotropy that arises with the potential $\mathcal{v}_{int}^{(2)}(\vec{r})$, whose Fourier transform is given by Eq. (4.16). As in Fig. 10, $x = 0$ represents the contribution only from the central-ion potential, in this case $\mathcal{v}_2(\vec{r})$, and $x = 1$ from $\mathcal{v}_s(\vec{r})$. Here, $G/E_F^0 = 0.35$ and the width of the K-ion po-

FIG. 10. Plot of the resistivity anisotropy and the resistivity in arbitrary units for $\mathcal{v}_{int}^{(1)}(\vec{r})$ as a function of x, the "concentration" of the potential $\mathcal{v}_1(\vec{r})$, for $G/E_F^0 = 0.35$ and $a = 1.0$. Results for both signs of β are shown, allowing for the cases of contraction and expansion of the lattice.
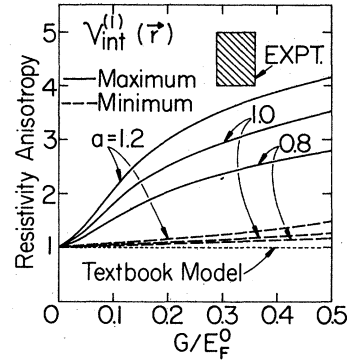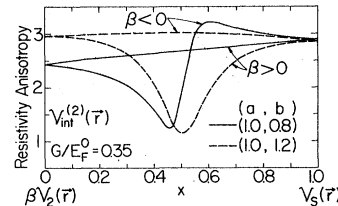

FIG. 12. Resistivity anisotropy using the potential $\mathcal{v}_2(\vec{r})$ as a function of x, with $G/E_F^0 = 0.35$. Here a is associated with the width of a K-ion potential and b with the width of the impurity potential. With $a = 1.0$ fixed, we choose values of b 20% larger and smaller than a. We include the possibilities of contraction or expansion of each case by including both signs of β.

tential is fixed by $a = 1.0$. We consider the two cases in which $b = 0.8$ or 1.2, that is, the width of the impurity ion potential is 20% larger or smaller than that of the K-ion potential. The case for $b = 0.8$ shown here has a very similar dependence on x as the example illustrated in Fig. 10. In addition, the shapes of the curves for the resistivity at $G = 0$ (not shown) for $\beta < 0$ and $\beta > 0$ are approximately the same, with minima at $x = 0.5$. However, here for $\beta < 0$ the ratio of the resistivity for $x = 0$ or $x = 1$ with respect to that for $x = 0.5$ is 35 to 1 as opposed to 8 to 1 for the analogous case in Fig. 10. For $b = 1.2$, the resistivity curve as a function of x is nearly identical to that for $b = 0.8$ except that the curves for $\beta < 0$ and $\beta > 0$ are interchanged. The anisotropy curve, with $G/E_F^0 = 0.35$, shown by the dashed curve, acquires a different shape. The large cancellation occurs for $\beta > 0$ and the function reaches a minimum and not a maximum. The $\beta < 0$ curve achieves a slight maximum. These shapes occur when the anisotropies due to $\mathcal{V}_s(\vec{r})$ and $\mathcal{V}_2(\vec{r})$ are almost the same. We will not show the variations of the maxima and minima as a function of G/E_F^0, as in Fig. 11. The shapes of such curves are the same as in Fig. 11. For all the combinations of parameters considered in Fig. 8, the maxima are somewhat smaller than those in Fig. 11 for the same values of a.

Preliminary results to those reported in this section appeared in Ref. 5. The curves displayed there correspond to those in Figs. 7, 9, and 11 of this paper with $a = 1.0$. The central-ion potential $\mathcal{V}_2(\vec{r})$ was not considered. The earlier curves showed slightly larger anisotropies due to various mathematical approximations in that work.

VII. CONCLUSIONS

We have seen that the results of induced-torque experiments on sample K-10 of Holroyd and Datars prove that K neither has a simply connected Fermi surface nor is of cubic symmetry. In addition, the data of Figs. 1 and 2 forces one to conclude that the residual resistivity in K is anisotropic by as large as a factor of 5 to 1. We have shown that the hypothesis of a CDW structure provides a quantitative explanation of this ratio. Although we do not attempt to explain the high-field torque anomalies here, the CDW clearly contains the features of a preferred axis and a multiply connected Fermi surface.

In this paper, we have not included any of the effects of phasons,[13,28] or phase modulations of the CDW, that might exist in K. It has recently been shown that electrons in the conical-point regions of the Fermi surface shown in Fig. 3 scatter strongly from phasons.[29] This would produce an additional enhancement of the umklapp scattering discussed here and would therefore increase the residual resistivity anisotropy that one would predict in the presence of a CDW. Although a CDW is expected to lead to weak diffraction satellites, phasons could reduce their intensity in K by several orders of magnitude.[14] As has been suggested in the past, an attempt should be made to search for these satellites at 10^{-7} of the (110) intensity level.

Variation in the results of torque data from sample to sample, which has led to much of the controversy discussed here, implies that a $\hat{Q}$-domain structure exists in most samples. The anisotropy in the resistivity tensor discussed in this paper would permit the residual resistivity to vary up to a factor of 4, depending on the distribution of orientations of $\vec{Q}$ in the domains. It is commonly found that in high-purity samples of K, the resistivity can vary by as much as a factor of 2 from run to run on the same sample, depending on how the sample is handled. As was first suggested in Ref. 5, the sample K-10 of Holroyd and Datars may be the first single $\hat{Q}$-domain sample ever studied. Perhaps this could be attributed to the fact that the sample was grown carefully in the smooth spherical kel-F mold and was kept protected by the mold throughout the course of the experiments. Clearly, induced-torque experiments could be used to characterize samples, so that at least one could determine whether a given sample were single $\hat{Q}$.

One of the main difficulties with the CDW model is the apparent contradiction with de Haas–van Alphen experiments.[9] These experiments imply that the Fermi surface is spherical to one part in 10^3. However, it is not clear whether this can be attributed to a multi-$\hat{Q}$-domain structure. On the other hand, results of recent de Haas–van Alphen experiments[30] show some of the effects expected on the basis of a CDW model. We emphasize the importance of performing de Haas–van Alphen experiments on a sample that exhibits the huge induced-torque anisotropies of Fig. 1 in order to resolve this dilemma.

[1]J. A. Schaefer and J. A. Marcus, Phys. Rev. Lett. **27**, 935 (1971).

[2]J. S. Lass, J. Phys. C **3**, 1926 (1970).

[3]J. S. Lass, Phys. Rev. B **13**, 2247 (1976).

[4]F. W. Holroyd and W. R. Datars, Can. J. Phys. **53**, 2517 (1975); and private communication.

[5]A preliminary exposition of this theory appeared in Marilyn F. Bishop and A. W. Overhauser, Phys. Rev. Lett. **39**, 632 (1977).

[6]L. D. Landau and E. M. Lifshitz, *Electrodynamics of Continous Media*, translated by J. B. Sykes and J. S. Bell (Pergamon, New York, 1960), p. 209.

[7]P. B. Visscher and L. M. Falicov, Phys. Rev. B **2**, 1518 (1970).

[8]A. W. Overhauser, Phys. Rev. Lett. **27**, 938 (1971).

[9]D. Shoenberg and P. J. Stiles, Proc. R. Soc. A **281**, 62 (1964); M. J. G. Lee and L. M. Falicov, *ibid.* **304**, 319 (1968).

[10]J. Monin and G. A. Boutry, Phys. Rev. B **9**, 1309 (1974).

[11]I. M. Lifshitz, M. Y. Azbel, and M. I. Kaganov, Zh. Eksp. Teor. Fiz. **31**, 63 (1956) [Sov. Phys.-JETP **4**, 41 (1957)].

[12]B. K. Jones, Phys. Rev. **179**, 637 (1969).

[13]However, because the kel-F mold was transparent, both Holroyd and Datars observed that it was completely filled. They also remarked that sample K-10 had a diameter of 1.11 cm (not 1.71), and that the ordinate scale of (their) Fig. 5(a) was incorrect. Magnet rotation rate for this spectrum was 22°/min (not 35°/min).

[14]For a review, see A. W. Overhauser, Phys. Rev. B **3**, 3173 (1971); or Adv. Phys. **27**, 343 (1978).

[15]A. W. Overhauser, Phys. Rev. Lett. **4**, 462 (1960); Phys. Rev. **128**, 1437 (1962).

[16]P. A. Smith and C. S. Smith, J. Phys. Chem. Solids **26**, 279 (1965).

[17]A. W. Overhauser, Phys. Rev. B **3**, 3173 (1971); **9**, 2441 (1974).

[18]A. W. Overhauser and R. L. Gorman, Phys. Rev. **102**, 676 (1956).

[19]J. D. Eshelby, J. Appl. Phys. **25**, 255 (1954); A. E. H. Love, *Mathematical Theory of Elasticity*, 4th ed. (Dover, New York, 1944), p. 187.

[20]T. M. Rice and L. J. Sham, Phys. Rev. B **1**, 4546 (1970).

[21]See, for instance, J. M. Ziman, *Principles of the Theory of Solids*, 2nd ed. (Cambridge U. P., London, 1972), Cahp. 7.

[22]J. M. Ziman, *Electrons and Phonons* (Oxford U.P., London, 1960), Sec. 7.3.

[23]Reference 20, Secs. 7.7 and 7.9.

[24]See, A. H. Wilson, *The Theory of Metals*, 2nd ed. (Cambridge U. P., London, 1953), Chap. 9.

[25]A. W. Overhauser, Phys. Rev. B **14**, 3371 (1976); and Phys. Rev. **156**, 844 (1967).

[26]A. W. Overhauser, Phys. Rev. **168**, 763 (1968).

[27]C. C. Grimes and A. F. Kip, Phys. Rev. **132**, 1991 (1963).

[28]A. W. Overhauser, Hyperfine Interactions **4**, 786 (1978).

[29]M. L. Boriack and A. W. Overhauser, Phys. Rev. B **17**, 4549 (1978).

[30]Z. Altounian, C. Verge, and W. R. Datars, J. Phys. F **8**, 75 (1978).